JOURNAL OF SYNCHROTRON RADIATION

ISSN 1600-5775

Hard X-rays for processing hybrid organic–inorganic thick films

Yu Jiang,[a] Davide Carboni,[a] Alessandra Pinna,[a] Benedetta Marmiroli,[b] Luca Malfatti[a] and Plinio Innocenzi[a]*

[a]Laboratorio di Scienza dei Materiali e Nanotecnologie, DADU, Università di Sassari, CR-INSTM, Palazzo Pou Salit, Piazza Duomo 6, 07041 Alghero (Sassari), Italy, and [b]Institute of Inorganic Chemistry, Graz University of Technology, Stremayrgasse 9/IV, 8010 Graz, Austria. *Correspondence e-mail: plinio@uniss.it

Received 31 July 2015
Accepted 5 October 2015

Edited by A. F. Craievich, University of São Paulo, Brazil

Keywords: hybrid organic–inorganic films; hard X-rays; nanoindentation; mechanical properties.

Hard X-rays, deriving from a synchrotron light source, have been used as an effective tool for processing hybrid organic–inorganic films and thick coatings up to several micrometres. These coatings could be directly modified, in terms of composition and properties, by controlled exposure to X-rays. The physico-chemical properties of the coatings, such as hardness, refractive index and fluorescence, can be properly tuned using the interaction of hard X-rays with the sol–gel hybrid films. The changes in the microstructure have been correlated especially with the modification of the optical and the mechanical properties. A relationship between the degradation rate of the organic groups and the rise of fluorescence from the hybrid material has been observed; nanoindentation analysis of the coatings as a function of the X-ray doses has shown a not linear dependence between thickness and film hardness.

1. Introduction

Hybrid organic–inorganic films are among the most successful examples of sol–gel materials and have been widely applied in several industrial products, such as anti-scratch (Zurlini *et al.*, 2009) and anti-corrosion (Guglielmi, 1997) coatings, optical films (Paquez *et al.*, 2015) and thermal barrier layers (Pin *et al.*, 2014). Some of the structural features of hybrid organic–inorganic films, such as their hydrophobicity, can be simply tailored by tuning the acidity of the sol (Carboni *et al.*, 2014). In other cases the use of hybrid precursors makes it possible to induce the formation of mesoporous crystalline structures with improved mechanical properties (Carboni *et al.*, 2015). The sol–gel films are deposited by different methods, such as spray-, spin- or dip-coating and can be thermally or UV cured (Van de Leest, 1995; Bohannan *et al.*, 2002). Just after the deposition, the films remain compliant enough because of their gel state to be easily patterned by different techniques (Innocenzi *et al.*, 2008, 2012, 2014). One of the most applied lithographic techniques for sol–gel films is UV-patterning which is a simple and very effective method. Another possibility is the exposure to soft (Brusatin *et al.*, 2008) and hard X-rays (Innocenzi *et al.*, 2011) which has shown to be a powerful lithographic tool to pattern thick films (Falcaro *et al.*, 2008, 2009). These techniques apparently cannot be competitive with UV lithography in terms of costs (Ma *et al.*, 2001; Lasagni *et al.*, 2005), because they may require a synchrotron radiation source. X-ray-based lithographies, however, are almost the only viable choice when specific requirements have to be fulfilled (Faustini *et al.*, 2011; Costacurta *et al.*, 2011). Soft X-rays, in particular, allow patterning with a high spatial

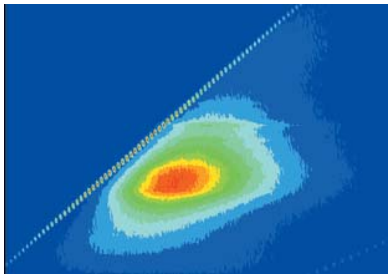

© 2016 International Union of Crystallography

resolution to be obtained, whilst hard X-rays, having a deep penetration within the material, allow writing on to very thick films with high aspect ratios (Ehrfeld *et al.*, 1999; Meyer *et al.*, 2008; Falcaro *et al.*, 2011 Malfatti *et al.*, 2010, 2011). The exposure of hybrid films to hard X-rays induces densification of the oxide component, through —OH condensation, and removal of the organic part. The extent of the two effects depends on the X-ray dose; higher doses produce a better condensation and faster removal of the organic. On the other hand, the exposure to X-ray radiation does not affect the films that remain defect free with an excellent optical grade. Another advantage of the combination of hard X-rays and hybrid films is that the direct exposure does not produce the typical phenomenon of bubbling observed at high doses in polymethylmethacrylate (De Carlo *et al.*, 1998) which could represent a severe limitation in applying deep X-ray lithography (DXRL) to polymeric materials (Costacurta *et al.*, 2010).

We have shown, in previous works, that the formation of free radicals is mainly responsible for the effects produced by hard X-rays on sol–gel films. Both the densification of M—OH and M—OR species (where M is a metal and R is an organic group), as well as the removal of organic molecules that are bound to silicon *via* the covalent Si—C bonds, have been attributed to free radicals generated by X-rays. The importance of free radicals, produced by the interaction of highly energetic photons with water and OH groups largely present in as-deposited sol–gel films, has been demonstrated by introducing a radical scavenger within a hybrid film (Pinna *et al.*, 2012). Given the capability of fullerene molecules to work as radical sinks, a fullerene-doped hybrid material has been exposed to hard X-rays produced by synchrotron radiation and its response has been compared with an un-doped sample. The fullerene-doped film has shown a lower condensation and lower degree of organic removal confirming that the radicals play a primary role in the structural modification of the material.

In the present work we have investigated the processing of hybrid films, characterized by a high content of organic moieties, exposed to hard X-rays. This is an important and challenging task for practical applications because, in general, when using the sol–gel route, a cumbersome multilayer deposition is necessary, even for obtaining a 1 µm-thick film. Another possibility is to use a hybrid film which can be deposited with a much higher thickness of up to some tens of microns. In this case, a silica film is obtained after removing the organic component by thermally treating the samples in air at temperatures higher than 773 K (Falcaro *et al.*, 2005).

Here we have reported the synthesis of silica hybrid films with a high content of methyl groups and exposed them to hard X-rays to condense the matrix and remove the organic moieties; the X-ray processing of the hybrid films has been studied as a function of X-ray doses. Interestingly, we have observed an outcome, *i.e.* the photoluminescence of the samples, which has not been observed before, neither in hybrid with lower methyl content nor in purely oxide sol–gel films (Innocenzi *et al.*, 2011).

2. Experimental

2.1. Chemicals

Tetraethylorthosilicate (TEOS) (Aldrich, 99% purity), methyltriethoxysilane (MTES) (Aldrich, 98% purity), ethanol (EtOH) (Fluka, >99.8%), hydrochloric acid (Sigma-Aldrich, 37% wt/wt) and water (milli-Q) are used. *p*-Type boron-doped, (100) cut, 381 mm-thick silicon wafers (Si-Mat) and silica slides were used as substrates for film deposition. The silicon wafers and silica slides were washed with water, acetone and then dried with compressed air before film deposition.

2.2. Synthesis of the precursor sols

The sol was prepared by mixing 2 ml EtOH, 3 ml MTES, 1 ml TEOS, 0.3 ml water and 0.2 ml hydrochloric acid (2 *M*) in a glass vial (molar ratios, MTES:TEOS:EtOH:H_2O:HCl = 3.4:1.0:7.7:3.7:0.1). The solution was stirred for 11 h at room temperature in a closed vial. Then 200 µl of milli-Q water was added to the hybrid sol (MTES–TEOS) and the solution was left to react under stirring for 1 h.

2.3. Synthesis of hybrid organic–inorganic films

The hybrid films were deposited by spin-coating onto silicon wafers and silica slides with a spinning rate of 500 r.p.m. for 30 s. The deposition was performed at 298 K and the films were then placed in an oven at 373 K for 1 h.

2.4. Hard X-rays exposure

After thermal treatment, the MTES–TEOS hybrid films were directly exposed to hard X-rays using the deep X-ray lithography beamline at the Elettra synchrotron facility (Trieste, Italy). Hard X-rays were obtained from the storage ring working at 2 GeV with a white beam of energy ranging from 2 to 20 keV. The energies per unit area incident to the sample surface were 188.5, 377, 754 and 1508 J cm^{-2}. During X-ray exposure, the samples were mounted on the top of a water-cooled stainless steel plate (scanner), which was kept in continuous motion to obtain a homogeneous exposure of areas larger than the beam size; the scanner rate was set to 20 mm s^{-1}.

2.5. Material characterization

Fourier-transform infrared (FTIR) spectroscopy analysis was performed with a Bruker infrared Vertex 70v interferometer. The spectra were recorded in transmission mode between 4000 and 400 cm^{-1} by averaging 256 scans with 4 cm^{-1} of resolution. A silicon wafer was used as the background; the baseline was fitted by a concave rubber band correction with *OPUS 7.0* software.

A Wollam-α spectroscopic ellipsometer with fixed angle geometry was used to estimate the thickness and refractive index dispersions of the hybrid films deposited on silicon substrates, by fitting the experimental data with a model for transparent films on Si substrates. The fit showed an average mean square error always lower than 6.5.

Transparency of the hybrid films was measured with a Nicolet Evolution 300 UV–Vis spectrophotometer in the range 200–800 nm with a bandwidth of 1.5 nm. A clean quartz slide was used as a background reference.

The hydrophobicity of the hybrid films was evaluated using a Dataphysics OCA 20 image capture system by measuring the contact angle of 5 µl water droplets deposited on the hybrid films coated on silicon substrates. The contact angle was taken as a median of at least five measurements.

Fluorescence spectra were measured using a Horiba Jobin Yvon FluoroMax-3 spectrofluorometer; three-dimensional mapping was performed with a 450 W xenon lamp as the excitation source. Three-dimensional maps were collected with an excitation range of 304−800 nm and an emission range of 315−800 nm with a 1 nm slit for both excitation and emission.

The nanoindentation analysis was performed using a CSM Table Top Nanoindentation Tester equipped with a head suitable for loadings from 0.1 up to 500 mN and a load resolution of 0.04 mN. The instrument is mounted on an anti-vibration support. The Young's modulus and penetration depth of the hybrid films were evaluated by using at least four measurements with a normal force of 0.8 mN as a function of the X-ray dose exposure, ranging from 0 to 1508 J cm^{-2}. The standard deviations of the values are also reported as error bars in the corresponding graphs.

3. Results and discussion

The structural modifications induced by X-ray irradiation in organic–inorganic materials have been studied using silica hybrid materials with a high content of methyl groups; these moieties, which are covalently attached to silicon through $-Si-CH_3$ bonds, cannot be hydrolysed during the sol–gel reactions but can modify the silica network structure and properties. We have, therefore, used a wide set of characterization techniques to correlate the structural modifications due to the exposure with the changes in the properties of the materials.

The thickness of the hybrid films exposed to increasing X-ray doses has been measured by spectroscopic ellipsometry (Fig. 1). The thickness decreases with a nonlinear trend from 2.6 µm (not-exposed film) down to 2.05 µm (1508 J cm^{-2} dose); the percentage of thickness reduction is also shown in Fig. 1 (right scale). By considering the change of film thickness as a function of the irradiation dose, we observe that the hard X-rays cause an almost linear thinning of the coatings up to 377 J cm^{-2}; above this threshold, the slope decrease shows that the coatings become less sensitive to the irradiation dose. In fact, X-rays affect the OH groups, which are contained in the not completely dense coatings. At higher doses the number of −OH groups is lower and, therefore, the films shrink less because the network is more and more cross linked (Soler-Illia *et al.*, 2012). The percentage of thickness reduction in Fig. 1 (right scale) shows that with respect to the not-exposed films the thickness decreases by 13% after exposing

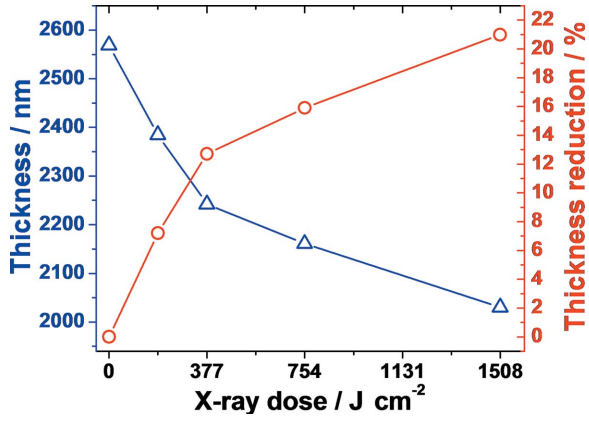

Figure 1
Absolute thickness (left *y* scale) and percentage of thickness reduction (right *y* scale) for silica hybrid films exposed to increasing hard X-ray doses (from 0 to 1508 J cm^{-2}).

the sample to 377 J cm^{-2} whilst the relative reduction is only 8% (21% overall reduction) when the sample is exposed to a fourfold dose (1508 J cm^{-2}).

Fig. 2(*a*) shows the dispersion of the refractive index, *n*, plotted in the 380–900 nm range. These data have been obtained as a fit of the Ψ and Δ ellipsometric parameters[1], considering the coatings as transparent films (Cauchy films). Higher-exposure doses induce an increase in the refractive index that grows monotonically from the not-exposed up to the 1508 J cm^{-2} exposed sample. Similarly to what was observed for the thickness, the trend for the refractive index also shows a slope variation above 377 J cm^{-2}. This can be better observed by plotting the refractive index at fixed wavelengths, 400 and 600 nm, at increasing X-ray doses (Fig. 2*b*).

The correlation between the structural changes and the structural properties of the hybrid films has been studied in detail using FTIR spectroscopy. The FTIR absorption spectra of the silica hybrid films exposed to increasing hard X-ray doses are shown in Fig. 3(*a*). The spectra are characterized by the presence of a wide absorption band peaking around 3400 cm^{-1} assigned to OH groups (OH symmetric stretching) which are hydrogen bonded to the oxygen of neighbouring silanols [ν_s(OH$\cdots$HOSi)] (Malfatti *et al.*, 2007). A sharp, less intense band at 3600 cm^{-1} is attributed to the presence of isolated and twin silanols groups (Innocenzi, 2003). The trend shown by these bands is quite unexpected because they increase in intensity with the dose whilst an opposite response has been observed previously in silica and hybrid films with a low content of methyl groups (Innocenzi *et al.*, 2011). On the other hand, the main silica band at 1073 cm^{-1} [ν_{as}(Si−O−Si)] increases in intensity with the dose, which is an indication of the proceeding silica backbone condensation at higher X-ray exposure values. To understand this peculiar material response, we have correlated the evolution of the 1275 cm^{-1}

[1] The ellipsometric parameters are defined by the equation $\tan(\Psi)\exp(i\Delta) = r_p/r_s$, where r_p and r_s are the reflectivity for *p*- and *s*-polarized light, respectively.

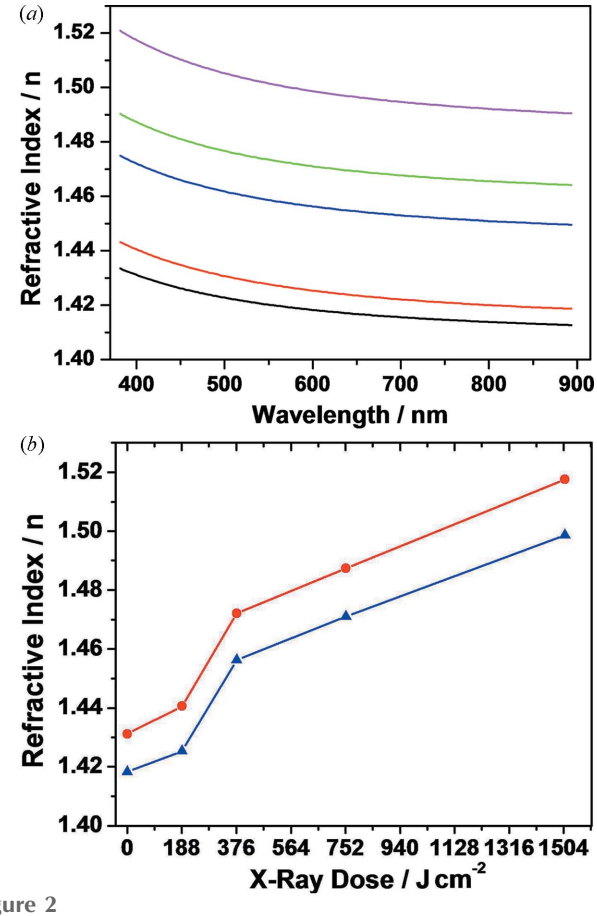

Figure 2
(*a*) Refractive index dispersion in the 380–900 nm range of silica hybrid films exposed to increasing hard X-ray doses, not exposed (black line), exposed to 188.5 (red line), 377 (blue line), 754 (green line) and 1508 J cm^{-2} (pink line). (*b*) Refractive index at 400 (red dots) and 600 nm (blue triangles) as a function of increasing X-ray doses. The lines are a guide for the eyes.

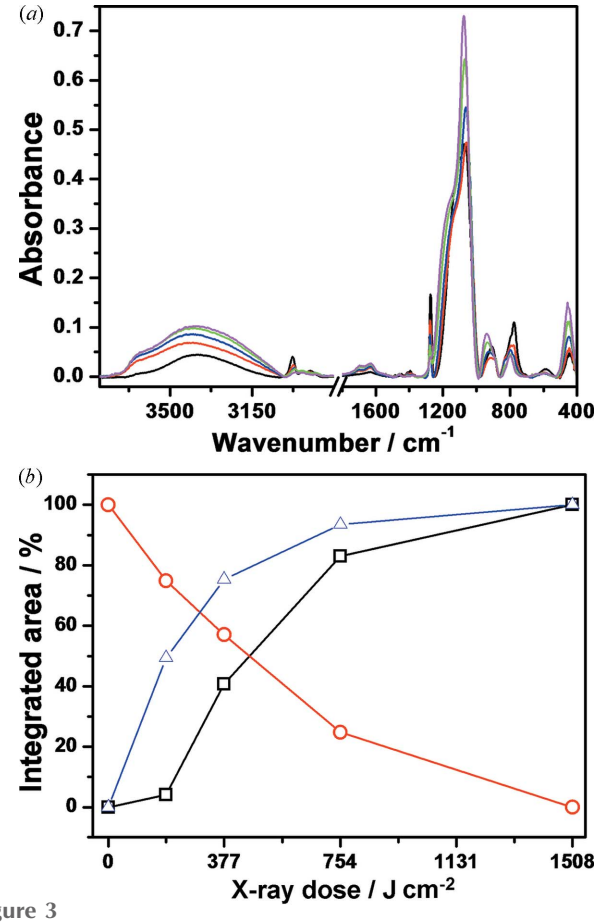

Figure 3
(*a*) FTIR spectra of silica hybrid films exposed to increasing hard X-ray doses: not exposed (black line), exposed to 188.5 (red line), 377 (blue line), 754 (green line) and 1508 J cm^{-2} (pink line). (*b*) Integrated area % of Si—O—Si group at 1073 cm^{-1} (black line), —CH_3 group at 1275 cm^{-1} (red line) and Si—OH bond at 3396 cm^{-1} (blue line) as a function of increasing X-ray doses. The lines are a guide for the eyes.

band [red line in Fig. 3(*b*)] assigned to methyl groups with those attributed to —OH and Si—O—Si groups, at 3396 and 1073 cm^{-1}, respectively [the blue and the black lines in Fig. 3(*b*)]. The interplay between these three functional groups follows a complex mechanism as it involves simultaneous and delayed interactions triggered by X-rays. As shown in our previous work (Innocenzi *et al.*, 2011), the residual water and the hydroxyl groups, which are present in the as-deposited films, produce upon X-ray exposure radical species that induce different chemical reactions. Radicals, in fact, promote the polycondensation of the siloxane oligomers and, at the same time, allow the degradation and the removal of the organic part of the hybrid matrix. This is realised by promoting an anaerobic stepwise oxidation of —Si—CH_3 into alcohol (—Si—CH_2-OH) first, then into aldehydes [—Si—C(O)H] and carboxy-derived structures [—Si—C(O)OH], and finally removing most of the organic moieties as CO_2, giving rise to new —Si—OH groups. The latter can further interact with the ionizing radiation to extend the Si—O—Si network. As a result of these interactions, the integrated areas of the bands related to hydroxyl, silanol and methyl groups follow nonlinear trends that allow some correlations to be established. Low doses, in fact, cause a remarkable removal of the organic groups from the matrix and an increase of the silanol groups. However, these changes do not find a counterpart in the increase of the polycondensation of the inorganic network. This is attributed to the fact that the degradation rate of the methyl group corresponds to the appearance of new transient organic species, intermediates of its oxidative degradation, and thus cannot match directly with the formation of free silanols. Moreover, the appearance of '*newbies*' —Si—OH promotes the formation of small oligomeric siloxanes that cannot be studied by following the band at 1073 cm^{-1}. A real strengthening of the siloxane backbone can be, in fact, observed only after reaching the 377 J cm^{-2} dose. Above this dose, whereas the CH_3 removal proceeds almost linearly, the increase of silanol content seems to be slowed down. This response can be explained by considering that, although the free Si—OH of the matrix undergoes condensation, more silanols are originated as a result of the final step of the oxidative degradation of the methyl groups. At this stage (754 J cm^{-2}), we have also observed the highest variation in the percentage of polycondensation of the matrix (from 40 to 80%), as deduced by the trend of the Si—O—Si band.

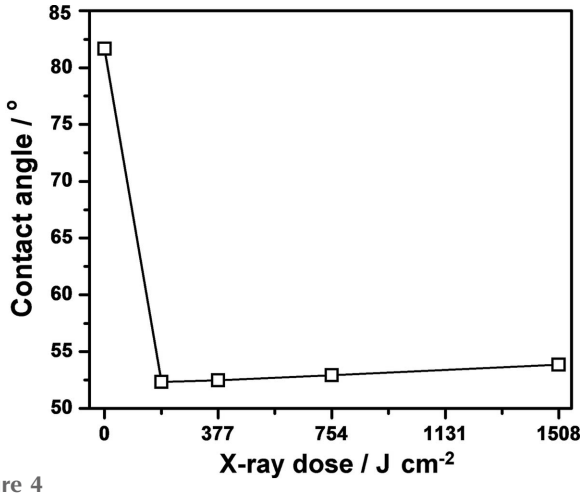

Figure 4
Contact angle of silica hybrid films as a function of increasing X-ray doses. The line is a guide for the eyes.

The complex chemical processes involved in the X-ray-induced densification of the coatings are also reflected in the contact angle measurements at increasing exposure times (Fig. 4). In the not-exposed film, the high concentration of methyl groups confers a certain degree of hydrophobicity to the matrix (83°). However, this angle undergoes to a sudden drop (−36%) after exposing the sample to the lowest dose (188.5 J cm^{-2}) (53°) and it is only marginally recovered with the increasing doses as a consequence of the densification of the Si—O—Si backbone, which reduces the hydrogen bonding capability and, therefore, the hydrophilicity, of the silica matrix.

The interaction of the hybrid organic–inorganic matrix with the hard X-rays does not affect only the chemistry of the materials but also the functional properties, such as the optical transmittance, the luminescence and the hardness. Fig. 5(*a*) shows that the transmittance of the films decreases in the UV range for increasing irradiation doses while the transmittance in the visible range is not affected. These changes can be better observed by considering the average transmittance, which is calculated over the whole range of wavelengths (Fig. 5*b*). This value reaches a minimum of 80% of the initial transmittance at the highest dose (1508 J cm^{-2}). This effect can be attributed to the formation of intermediate species coming from the oxidative degradation of the methyl groups in the hybrid coatings that form amorphous sp^3 carbon clusters (Pivin & Colombo, 1997; Pivin *et al.*, 2003).

More interestingly, the interaction of the hybrid organic–inorganic matrix with the ionizing radiation allows the tuning of the photoluminescence properties of the films. The three-dimensional fluorescence maps (emission–excitation–intensity) in Fig. 6 show that at low doses the hard X-rays trigger the photoluminescence of the matrix, whereas above 754 J cm^{-2} the photoluminescence is quenched. This property has been correlated to the presence of organic groups or carbon clusters derived from the degradation of $-CH_3$. Unlike the trend observed in the optical absorption that increases linearly with the irradiation dose, the photo-

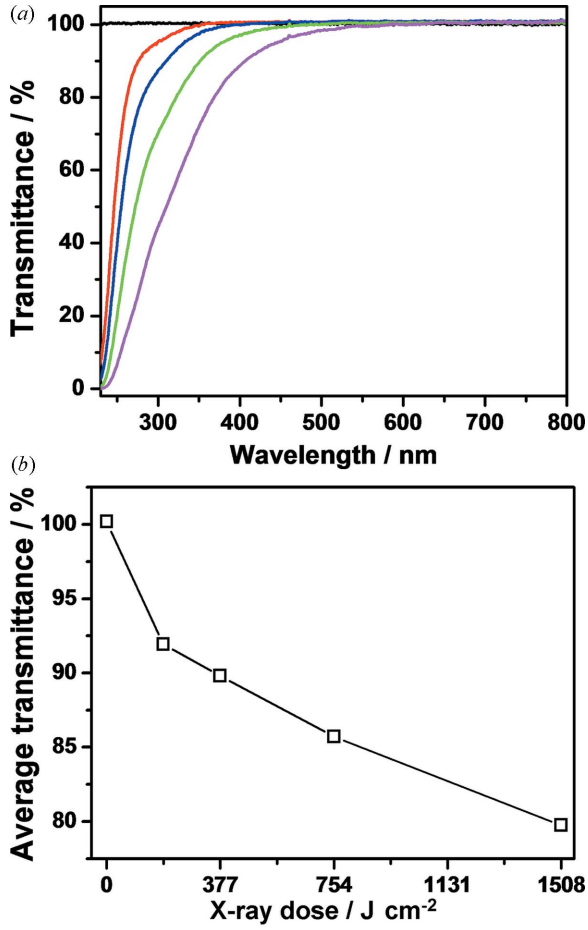

Figure 5
(*a*) UV–Vis transmittance spectra of silica hybrid films exposed to increasing hard X-ray doses: not exposed (black line), exposed to 188.5 (red line), 377 (blue line), 754 (green line) and 1508 J cm^{-2} (pink line). (*b*) Average transmittance of the silica hybrid films calculated in the range 230–800 nm as a function of increasing X-ray doses. The line is a guide for the eyes.

luminescence shows a maximum in intensity followed by a sudden decrease. This trend has been already observed in hybrid siloxanes polymers exposed to ion irradiation and attributed to the growth of carbon clusters, which induces a shift towards lower energy and a decrease of the radiative de-excitation probability with respect to nonradiative processes (Pivin & Sendova-Vassileva, 1998; Kumar *et al.*, 2005).

The film densification obtained by X-ray irradiation has also been assessed in terms of surface hardness. This is the first time, to our knowledge, that the mechanical properties of hybrid organic–inorganic sol–gel films have been measured as a function of the exposure to X-rays. Fig. 7(*a*) shows the representative loading and unloading curves obtained from the coatings exposed at increasing doses. The measurements have been performed using a constant loading equal to 0.8 mN to keep the penetration depth below 20% of the whole film thickness, thus avoiding the contribution of the substrate. The densification effect can be clearly observed as the penetration depth of the indenter dramatically decreases from the not-exposed (400 nm) up the 1508 J cm^{-2} exposed sample

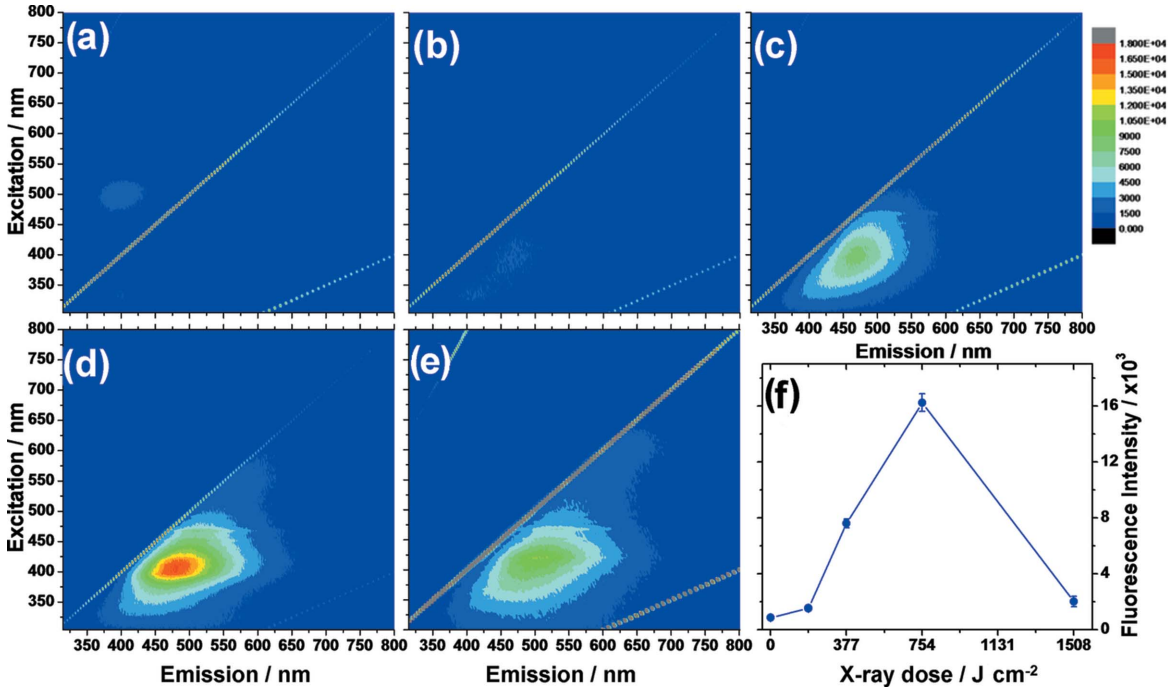

Figure 6
(*a*)–(*e*) Three-dimensional fluorescence maps of silica hybrid films exposed to increasing X-ray doses (0, 188.5, 377, 754 and 1508 J cm^{-2}). (*f*) Maxima of fluorescence intensity as a function of increasing X-ray doses.

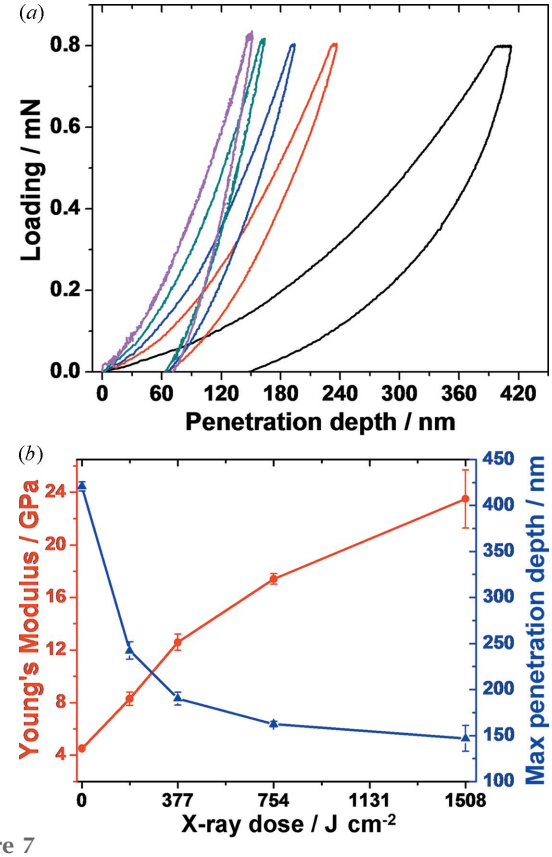

Figure 7
(*a*) Nanoindentation profiles of silica hybrid films exposed to increasing X-ray doses and performed with a constant loading force of 0.8 mN: not exposed (black line), exposed to 188.5 (red line), 377 (blue line), 754 (green line) and 1508 J cm^{-2} (pink line). (*b*) Young's modulus (red dots) and maximum penetration depth (blue triangles) of silica hybrid films as a function of increasing X-ray dose. The lines are a guide for the eyes.

(150 nm). The measurements have also allowed the Young's modulus (E) of the coatings to be estimated by fitting the indentation profile and by calculating the slope of the curve in a specific range (Fig. 7*b*). The E value ranges from 4.5 (not exposed) up to 23.5 GPa (1508 J cm^{-2}) reaching a remarkable absolute value for a hybrid organic–inorganic film (Mackenzie *et al.*, 1996; Latella *et al.*, 2003). The deposition of a sol with a high ratio of organic groups has allowed a quite thick film (2.57 µm) to be deposited which, after exposure to the highest X-ray dose, is still 2.03 µm thick. The final thickness and the corresponding remarkable E value are thus related to the almost complete disappearance of the organic moieties and the largely inorganic nature of the resulting coating.

4. Conclusions

The exposure of a methyl-based hybrid organic–inorganic film to hard X-rays induces a modification of structure and properties which depends on the extent of the residual organic groups and the condensation of the inorganic network. The chemo-physical properties have shown to be dependent on the exposure dose, which affects the optical and mechanical properties. The films become fluorescent upon X-ray exposure because of the presence of organic species derived by the partial degradation of the methyl groups. The removal of methyl groups and their by-products at high X-ray doses causes a quenching of the photoluminescence. The mechanical properties, such as the Young's modulus, show also a strong dependence on X-ray dose with a remarkably high value for the hybrid coating exposed to the higher dose.

The exposure of hybrid films to hard X-rays has shown to be a very effective tool for the design of the material properties that can be tuned as a function of the exposure dose.

Acknowledgements

The Sardinian Regional Government (RAS) is kindly acknowledged for funding D. Carboni through POR SARDEGNA FSE 2007–2013 – Obiettivo competitività regionale e occupazione, Asse IV Capitale umano, Linea di Attività l.3.1.

References

Bohannan, E. W., Gao, X. R., Gaston, K. R., Doss, C. D., Sotiriou-Leventis, C. & Leventis, N. (2002). *J. Sol.-Gel Sci. Technol.* **23**, 235–245.

Brusatin, G., Della Giustina, G., Romanato, F. & Guglielmi, M. (2008). *Nanotechnology*, **19**, 175306.

Carboni, D., Pinna, A., Malfatti, L. & Innocenzi, P. (2014). *New J. Chem.* **38**, 1635–1640.

Carboni, D., Pinna, A., Amenitsch, H., Casula, M. F., Loche, D., Malfatti, L. & Innocenzi, P. (2015). *Phys. Chem. Chem. Phys.* **17**, 10679–10686.

Costacurta, S., Falcaro, P., Malfatti, L., Marongiu, D., Marmiroli, B., Cacho-Nerin, F., Amenitsch, H., Kirkby, N. & Innocenzi, P. (2011). *Langmuir*, **27**, 3898–3905.

Costacurta, S., Malfatti, L., Patelli, A., Falcaro, P., Amenitsch, H., Marmiroli, B., Grenci, G., Piccinini, M. & Innocenzi, P. (2010). *Plasma Process. Polym.* **7**, 459–465.

De Carlo, F., Mancini, D. C., Lai, B. & Song, J. J. (1998). *Microsyst. Technol.* **4**, 86–88.

Ehrfeld, W., Hessel, V., Löwe, H., Schulz, C. & Weber, L. (1999). *Microsyst. Technol.* **5**, 105–112.

Falcaro, P., Costacurta, S., Malfatti, L., Buso, D., Patelli, A., Schiavuta, P., Piccinini, M., Grenci, G., Marmiroli, B., Amenitsch, H. & Innocenzi, P. (2011). *ACS Appl. Mater. Interfaces*, **3**, 245–251.

Falcaro, P., Costacurta, S., Malfatti, L., Takahashi, M., Kidchob, T., Casula, M. F., Piccinini, M., Marcelli, A., Marmiroli, B., Amenitsch, H., Schiavuta, P. & Innocenzi, P. (2008). *Adv. Mater.* **20**, 1864–1869.

Falcaro, P., Costacurta, S., Mattei, G., Amenitsch, H., Marcelli, A., Guidi, M. C., Piccinini, M., Nucara, A., Malfatti, L., Kidchob, T. & Innocenzi, P. (2005). *J. Am. Chem. Soc.* **127**, 3838–3846.

Falcaro, P., Malfatti, L., Vaccari, L., Amenitsch, H., Marmiroli, B., Grenci, G. & Innocenzi, P. (2009). *Adv. Mater.* **21**, 4932–4936.

Faustini, M., Marmiroli, B., Malfatti, L., Louis, B., Krins, N., Falcaro, P., Grenci, G., Laberty-Robert, C., Amenitsch, H., Innocenzi, P. & Grosso, D. (2011). *J. Mater. Chem.* **21**, 3597–3604.

Guglielmi, M. (1997). *J. Sol.-Gel Sci. Technol.* **8**, 443–449.

Innocenzi, P. (2003). *J. Non-Cryst. Solids*, **316**, 309–319.

Innocenzi, P., Kidchob, T., Falcaro, P. & Takahashi, M. (2008). *Chem. Mater.* **20**, 607–614.

Innocenzi, P., Malfatti, L. & Falcaro, P. (2012). *Soft Matter*, **8**, 3722–3729.

Innocenzi, P., Malfatti, L., Kidchob, T., Costacurta, S., Falcaro, P., Marmiroli, B., Cacho-Nerin, F. & Amenitsch, H. (2011). *J. Synchrotron Rad.* **18**, 280–286.

Innocenzi, P., Malfatti, L., Marmiroli, B. & Falcaro, P. (2014). *J. Sol.-Gel Sci. Technol.* **70**, 236–244.

Kumar, A., Singh, F., Pivin, J. C. & Avasthi, D. K. (2005). *Radiat. Meas.* **40**, 785–788.

Lasagni, A. S., Seyler, M., Holzapfel, C., Maier, W. F. & Mücklich, F. (2005). *Adv. Mater.* **17**, 2228–2232.

Latella, B. A., Ignat, M., Barbé, C. J., Cassidy, D. J. & Bartlett, J. R. (2003). *J. Sol.-Gel Sci. Technol.* **26**, 765–770.

Ma, J. H., Wu, G. M., Shen, J. & Wang, J. (2001). *J. Inorg. Mater.* **16**, 1174–1180.

Mackenzie, J. D., Huang, Q. & Iwamoto, T. (1996). *J. Sol-Gel Sci. Technol.* **7**, 151–161.

Malfatti, L., Falcaro, P., Marmiroli, B., Amenitsch, H., Piccinini, M., Falqui, A. & Innocenzi, P. (2011). *Nanoscale*, **3**, 3760–3766.

Malfatti, L., Kidchob, T., Falcaro, P., Costacurta, S., Piccinini, M., Guidi, M. C., Marcelli, A., Corrias, A., Casula, M. F., Amenitsch, H. & Innocenzi, P. (2007). *Micropor. Mesopor. Mater.* **103**, 113–122.

Malfatti, L., Marongiu, D., Costacurta, S., Falcaro, P., Amenitsch, H., Marmiroli, B., Grenci, G., Casula, M. F. & Innocenzi, P. (2010). *Chem. Mater.* **22**, 2132–2137.

Meyer, P., Schulz, J., Hahn, L. & Saile, V. (2008). *Microsyst. Technol.* **14**, 1491–1497.

Paquez, X., Amiard, G., de Combarieu, G., Boissière, C. & Grosso, D. (2015). *Chem. Mater.* **27**, 2711–2717.

Pin, L., Vidal, V., Blas, F., Ansart, F., Duluard, S., Bonino, J.-P., Le Maoult, Y. & Lours, P. (2014). *J. Eur. Ceram. Soc.* **34**, 961–974.

Pinna, A., Malfatti, L., Piccinini, M., Falcaro, P. & Innocenzi, P. (2012). *J. Synchrotron Rad.* **19**, 586–590.

Pivin, J. C. & Colombo, P. (1997). *J. Mater. Sci.* **32**, 6163–6173.

Pivin, J. C., Colombo, P., Martucci, A., Sorarù, D., Pippel, E. & Sendova-Vassileva, M. (2003). *J. Sol-Gel Sci. Technol.* **26**, 251–255.

Pivin, J. C. & Sendova-Vassileva, M. (1998). *Solid State Commun.* **106**, 133–138.

Soler-Illia, G. J. A. A., Angelomé, P. C., Fuertes, M. C., Grosso, D. & Boissière, C. (2012). *Nanoscale*, **4**, 2549–2566.

Van de Leest, R. E. (1995). *Appl. Surf. Sci.* **86**, 278–285.

Zurlini, P., Lorenzi, A., Alfieri, I., Gnappi, G., Montenero, A., Senin, N., Groppetti, R. & Fabbri, P. (2009). *Thin Solid Films*, **517**, 5881–5887.